Int J Thermophys (2007) 28:1026–1036
DOI 10.1007/s10765-007-0219-6

Thermophysical Properties of γ-Titanium Aluminide: The European IMPRESS Project

I. Egry · R. Brooks · D. Holland-Moritz · R. Novakovic · T. Matsushita · E. Ricci · S. Seetharaman · R. Wunderlich · D. Jarvis

Published online: 21 August 2007

Abstract In the framework of its 6th Framework Programme, the European Union funds the Integrated Project IMPRESS, related to industrial applications of Ti–Al and Ni–Al alloys. One central task of this project is the precise determination of the relevant thermophysical properties of selected alloys for both the solid and liquid phases. The properties to be measured include thermal data such as heat of fusion, specific heat, and thermal conductivity, as well as thermophysical and transport properties such as density, surface tension, and viscosity. In addition to conventional high-temperature equipment, containerless methods are used. This article introduces the IMPRESS project, and discusses the first results obtained to date.

Keywords Thermophysical properties · Titanium aluminides

I. Egry (✉)· D. Holland-Moritz
Institute for Materials Physics in Space, German Aerospace Center, 51170 Cologne, Germany
e-mail: Ivan.Egry@dlr.de

R. Brooks
Division of Materials Metrology, National Physical Laboratory, Teddington TW11 0LW, UK

R. Novakovic · E. Ricci
Institute for Energetics and Interfaces, Via De Marini 6, Genova 16149, Italy

T. Matsushita · S. Seetharaman
Department of Materials & Engineering, Division of Metallurgy, Royal Institute of Technology, Brinellvägen 23, Stockholm 10044, Sweden

R. Wunderlich
Materials Division, University of Ulm, Albert-Einstein-Allee 47, Ulm 89081, Germany

D. Jarvis
European Space Agency, Keplerlaan 1, Noordwijk 2201, Netherlands

1 Introduction

IMPRESS is an acronym for *I*ntermetallic *M*aterials *P*rocessing in *R*elation to *E*arth and *S*pace *S*olidification [1]. This project was selected by the European Commission as an Integrated Projected in its 6th Framework Programme, and started in November 2004. The main scientific objective of IMPRESS is to gain a better understanding of the links between materials processing routes, structure, and final properties of intermetallic alloys. Technically speaking, the project aims to develop and test two distinct prototypes based on intermetallic materials, namely,

(a) 40 cm cast γ-TiAl turbine blades for aero-engines and stationary gas turbines
(b) $<20\,\mu$m-sized Raney-type Ni–Al catalytic powder for use in hydrogen fuel cell electrodes and hydrogenation reactions.

Within the IMPRESS project, the measurement of thermophysical properties plays a central role, linking the experimental work and the modeling.

The main objectives of this work were first to define a measurement plan and, second to experimentally determine a first set of thermophysical property data for high-temperature melts of a selected TiAl/Ni–Al-based alloy. This set includes density, thermal expansion, enthalpy, specific heat, thermal diffusivity, electrical resistivity, and surface tension. The present work also includes an investigation of the influence of the surrounding atmosphere on thermophysical property measurements, e.g., the influence of different oxygen content in the working atmosphere on the surface tension.

At the beginning of the IMPRESS project, the exact composition of the γ-Ti–Al was defined. The challenge was to develop a castable alloy, free of grain refiners, like boron, and susceptible to heat treatment. Finally, a ternary Ti–Al–Nb alloy was chosen, which is the subject of thermophysical property measurements reported here. The nominal composition, in at%, is as follows: $Al_{45.5}Ti_{46.5}Nb_8$. Work on the Raney-type Ni–Al catalytic materials is not reported here.

2 Measurements

2.1 DSC Measurements

Thermal analysis was performed in a high temperature differential scanning calorimeter (HTDSC) (Netzsch Jupiter STA 449) with a maximum temperature of 1,650°C.

Calorimetry in the two-phase region and in the liquid phase up to temperatures of $T = 1{,}610$°C is complicated by the high chemical reactivity of TiAlNb affecting enthalpy measurements, and—due to possible changes in the composition—the observed transition temperatures. Experiments were performed in Pt-cups with Y_2O_3-coated alumina inlays. This combination showed the least reaction between the specimen and the container.

The specific heat capacity in the solid phase from $T = 400$–$1{,}430$°C of TiAlNb, is shown in Fig. 1. It can be fitted with the following cubic polynomial:

$$c_P(T) = 0.6324 + 7.44 \times 10^{-5} T - 2.07 \times 10^{-7} T^2 + 2.97 \times 10^{-10} T^3 \qquad (1)$$

with c_p in $J \cdot K^{-1} \cdot g^{-1}$ and T in °C.

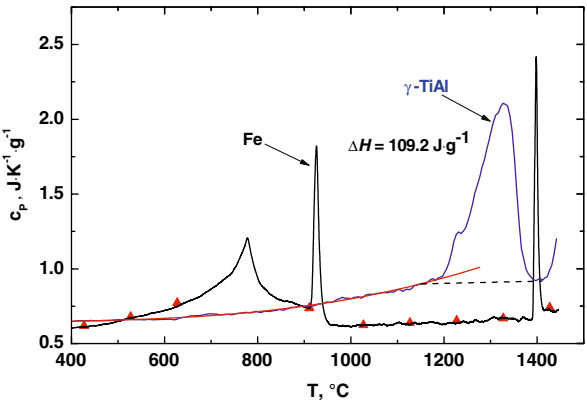

Fig. 1 Specific heat capacity in the solid phase of a TiAlNb specimen and corresponding values for an Fe-calibration standard. Triangles indicate standard c_p-values for Fe

In addition, the specific heat capacity of a high-purity Fe-calibration specimen of comparable thermal load and shape obtained directly after the TiAlNb measurement is shown. The triangles represent the standard values for Fe. The temperature calibration is obtained from the iron $\alpha \rightarrow \gamma$ and $\gamma \rightarrow \delta$ phase transitions at $T = 911°C$ and $T = 1{,}394°C$, respectively. For all specific-heat-capacity measurements with TiAlNb, consecutive calibration experiments with an Fe-standard were performed. The endothermal event in the TiAlNb thermogram with onset at $T = 1{,}195$–$1{,}401°C$ is identified with the $\alpha_2 + \gamma \rightarrow \alpha + \gamma$ phase transition. The enthalpy is $\Delta H_{tr} = 109.2\ \mathrm{J{\cdot}g^{-1}}$.

Values of the onset of melting, and of the enthalpy of fusion were determined as follows:

$$T_s = 1,500 \pm 5°C, \quad \Delta H_f = 340.2 \pm 3\mathrm{J} \cdot \mathrm{g}^{-1}.$$

This value of the enthalpy of fusion, is different from a value of $\Delta H_f = 411.5\ \mathrm{J} \cdot \mathrm{g}^{-1}$ obtained by rapid heating techniques [2] for a Ti44Al8Nb1B alloy.

Heating-rate-dependent measurements have been performed to identify the equilibrium liquidus temperature. From extrapolating the values shown in Fig. 2 to a zero heating rate, a value of $T_l = 1572.8 \pm 5°C$ is obtained.

For all phase transitions the fraction transformed has been evaluated on heating and cooling for rates of $R_C = 10$ and $20°C{\cdot}\mathrm{min}^{-1}$. An example of the $\alpha_2 + \gamma \rightarrow \alpha + \gamma$ transition on heating with $R_H = 20°C{\cdot}\mathrm{min}^{-1}$ is shown in Fig. 3.

The dashed curve represents a Boltzmann-type sigmoidal fit given by

$$y(x) = A_2 \left(1 - \frac{1}{1 + \exp[(x - x_o)/\mathrm{d}x]}\right) \tag{2}$$

x_o corresponds approximately to the temperature of 50% transformed. The difference of x_o values on heating and cooling in temperature scaling represents undercooling. The parameters A_2, x_o, and $\mathrm{d}x$ for the $\alpha_2 + \gamma \rightarrow \alpha + \gamma$ transition on heating with $R_H = 20\ °C{\cdot}\mathrm{min}^{-1}$ are as follows: $A_2 = 111.4$, $x_0 = 1006.5°C$, $\mathrm{d}x = 27.8°C$.

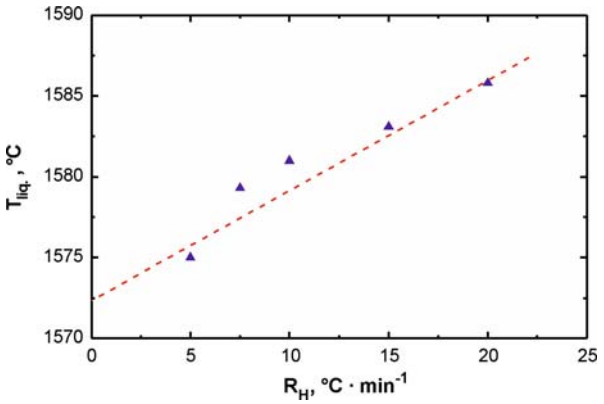

Fig. 2 Apparent liquidus temperature of TiAlNb-alloy as a function of heating rate

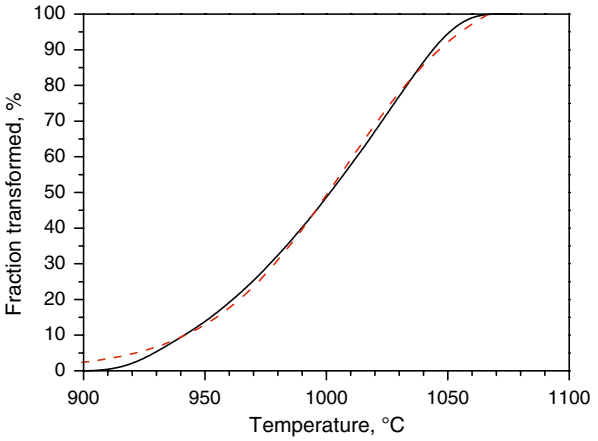

Fig. 3 Fraction transformed during $\alpha_2 + \gamma \rightarrow \alpha + \gamma$ transformation of TiAlNb as a function of temperature. Heating at $R_H = 20°C{\cdot}min^{-1}$. Dashed curve: Boltzmann type sigmoidal fit, Eq. 2

2.2 Laser-Flash Measurements

The thermal-diffusivity measurements were carried out as a round-robin exercise between NPL and KTH. Both labs used the laser-flash method (NPL: Netzsch 475, KTH: Shinku-Riko, TC-7000H/MELT). The heating and cooling rates were 10 and 6 K·min^{-1}, respectively. The thermal diffusivity was measured in the solid phase from room temperature to 1,300°C on heating and cooling, and is shown in Fig. 4. Full circles represent the measurement results in the heating cycle, and open circles represent the results for the cooling cycle. The results are fitted with a third-order polynomial, and the average between heating and cooling is taken as the recommended value:

$$\alpha = -3.01 \times 10^{-9}T^3 - 4.30 \times 10^{-7}T^2 + 5.18 \times 10^{-3}T + 5.36 \quad (20°C < T < 1300°C) \tag{3}$$

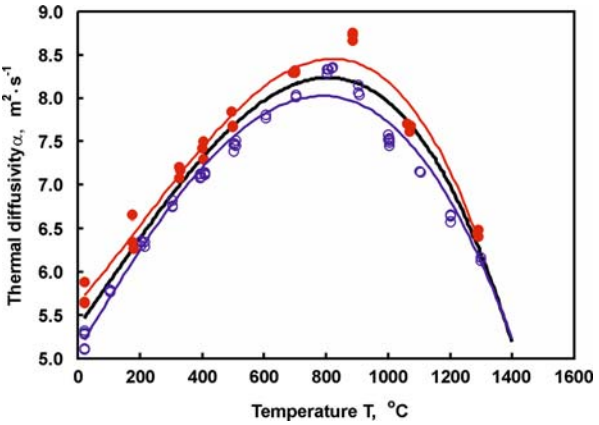

Fig. 4 Thermal diffusivity of TiAlNb alloy. Full and open circles correspond to heating and cooling, respectively. Bold line represents recommended values

2.3 Density

Thermal expansion measurements were carried out from room temperature to 1,300°C using a Linseis dilatometer. The first run showed a difference between heating and cooling behavior which is likely to be the effect of annealing the sample. Two further runs were carried out on the same sample, and the agreement between heating and cooling in these cases was far better, indicating a fully annealed specimen. The data show a minor change in slope at about 750°C, which can also be found for the electrical-resistivity data, and is observed for the thermal-diffusivity data at 800°C. A more noticeable deviation occurs at 1,200°C, which is also seen in the electrical-resistivity values. These are likely to be associated with phase changes, although detailed metallography has not been carried out on specimens quenched from these temperatures. In Table 1, results are provided for the coefficient of thermal expansion, i.e., the slope of the thermal expansion between 21.5°C and the temperature T, and the expansivity, i.e., the tangent to the thermal expansion at temperature T. The density of the solid alloy is determined from the room-temperature density and the thermal expansion and is shown in Fig. 5.

The density of the stable and deeply undercooled liquid phase has been investigated by the levitated drop method. The temperature of the samples is contactlessly measured with a one-color pyrometer. In order to determine the density of the melt, the samples were illuminated by a He–Ne laser beam and the shadowgraph of the sample is recorded by the use of a CCD camera. Under the assumption that the shape of the specimen is axially symmetric, the density of the melt is inferred from the edge profile of the shadowgraph. The experimental setup and the data evaluation procedure are described in detail in Ref. [3]. The results of the investigations obtained for two different samples are shown in Fig. 6, together with earlier data on the Ti44Al8Nb1B alloy [2]. A broad temperature range is covered ranging from 1,310 up to 1,675°C (T_L = 1,573°C).

Table 1 Thermal expansion, expansivity, and density of solid Ti–Al–Nb

Temp. (°C)	Mean expan. coeff. (10^{-6}°C^{-1})	Expansivity (10^{-6}°C^{-1})	Density ($Mg{\cdot}m^{-3}$)
21.5	–	–	4.213
50	8.9	–	4.210
100	9.8	10.5	4.203
150	10.1	10.4	4.197
200	10.1	10.6	4.190
250	10.3	11.2	4.183
300	10.5	11.4	4.176
350	10.7	11.6	4.169
400	10.8	11.7	4.162
450	10.9	12.0	4.154
500	11.0	12.2	4.147
550	11.1	12.4	4.139
600	11.3	12.6	4.132
650	11.4	12.9	4.124
700	11.5	13.2	4.116
750	11.6	13.4	4.108
800	11.7	13.7	4.099
850	11.9	14.0	4.091
900	12.0	14.6	4.082
950	12.2	15.4	4.073
1000	12.4	16.1	4.064
1050	12.5	16.9	4.054
1100	12.8	18.1	4.044
1150	13.0	20.0	4.032
1200	13.4	25.3	4.020
1250	14.0	36.5	4.002
1300	15.2	–	3.977

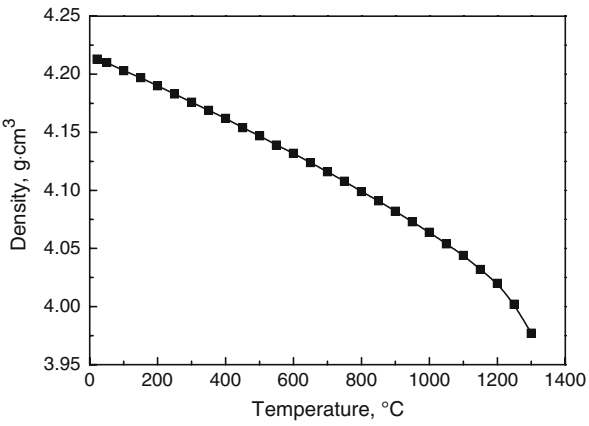

Fig. 5 Density of solid Ti–Al–Nb as a function of temperature

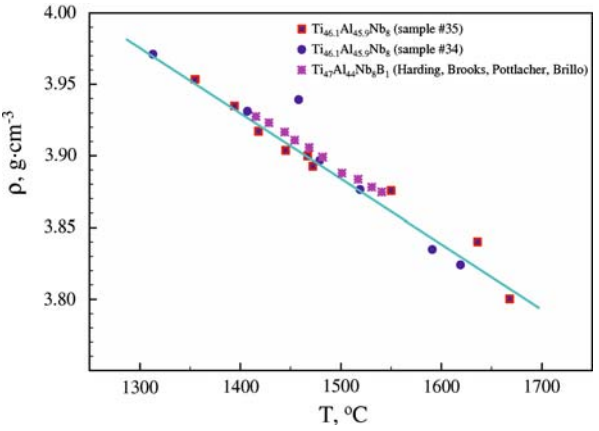

Fig. 6 Density of liquid TiAlNb as a function of temperature

The temperature dependence of the density of the liquid TiAlNb alloy is described by the following linear fit:

$$\rho = \rho(T_\mathrm{L}) + m(T - T_\mathrm{L}) \tag{4}$$
$$\rho(T_\mathrm{L}) = 3.85 \pm 0.03\ \mathrm{g \cdot cm^{-3}}, \quad m = (-4.57 \pm 0.19) \times 10^{-4} \mathrm{g \cdot cm^{-3} \cdot^{\circ} C^{-1}}$$

2.4 Surface Tension

The surface tension of stable and undercooled liquid TiAlNb is measured by use of the same electromagnetic levitation device that was also utilized for the density measurements described above. For determination of the surface tension, the oscillating droplet method [4] is applied. The oscillations of the sample surface are recorded from the top of the levitator with a video camera at a frame rate of 400 Hz with a resolution of $1,024 \times 1,000$ pixels. At each investigated temperature, a series of 4096 frames is acquired.

From the video sequences, frequency spectra of the sample radius, R, are determined. The spectrum contains five peaks at frequencies ω_i (i $= -2, -1, 0, 1, 2$) resulting from the surface oscilations. Moreover, three translational frequencies T_x, T_y, and T_z can be identified.

From the five surface oscillation frequencies and the three translational frequencies the surface tension, γ, is determined by use of the formula by Cummings and Blackburn [5]:

$$\gamma = \frac{3M}{160\pi} \sum_{m=-2}^{2} \omega_i^2 - 1.9\Omega^2 - 0.3 \left(\frac{g}{a}\right)^2 \Omega^{-2} \tag{5}$$

$$\text{with } \Omega^2 = \frac{1}{3}(T_x^2 + T_y^2 + T_z^2) \tag{6}$$

Here M denotes the sample mass.

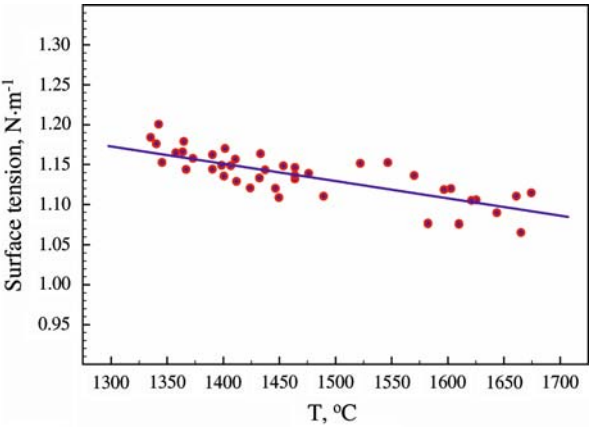

Fig. 7 Surface tension of liquid TiAlNb as a function of temperature. Line is a linear fit to the data

Fig. 8 Electrical resistivity of TiAlNb in the solid phase

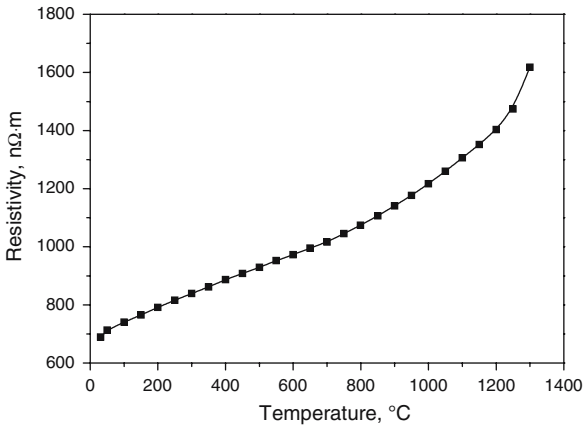

Figure 7 shows the measured surface tension as a function of temperature. Its temperature dependence is described by the following linear fit:

$$\gamma = \gamma(T_{\mathrm{L}}) + m(T - T_{\mathrm{L}}) \tag{7}$$
$$\gamma(T_{\mathrm{L}}) = (1.114 \pm 0.05)\mathrm{N} \cdot \mathrm{m}^{-1}, \quad m = (-2.17 \pm 0.3) \times 10^{-4}\mathrm{N} \cdot \mathrm{m}^{-1} \cdot^{\circ} \mathrm{C}^{-1}$$

2.5 Electrical Resistivity

Electical-resistivity measurements were carried out in a miniature ETMT (electrothermal mechanical testing) apparatus [6]. The sample is heated by a dc current and, via two thermocouple wires welded to the sample, a four-probe resistance measurement is taken. The heating rate is 5°C per second. An initial resistance measurement is made at room temperature. The results are given in Fig. 8. The data can be fitted by the following cubic expression for $20^{\circ}\mathrm{C} < T < 1,300^{\circ}\mathrm{C}$:

$$\rho(T) = 665.88 + 0.79T - 8.16 \times 10^{-4}T^2 + 5.72 \times 10^{-3}T^3 \text{n}\Omega \cdot \text{m} \qquad (8)$$

The measurements ended when the platinum thermocouple wires (Pt/Pt + 13%Rh) detached from the sample. This was caused by the melting of the wire as it reacted to form a Ti-Pt eutectic. Although not shown in Fig. 8, the onset of this process can be observed at the highest temperatures of the tests as an apparent decrease in the resistivity.

2.6 Thermodynamic Modeling

In order to understand better the mixing properties of the Al–Ti–Nb alloy system, particular attention was dedicated to the Al–Ti system and to the effect of a third component, Nb, on it. The thermophysical properties of the binary Al–Ti liquid alloy system have been investigated by a simple structural model for the chemical complexes (CFM) [7] as well as by the quasi-chemical approximation (QCA) [8] for a regular solution. In this way the effect of a short-range-order phenomenon on the surface properties of Al-Ti liquid alloys can be estimated by the difference in the surface composition or surface tension calculated by the two models.

Available experimental data on the thermodynamic properties as well as phase diagram information have been used for the calculation of order energy parameters for the liquid phase in the Al–Ti system. For all temperatures the mixing functions, i.e., the Gibbs free energies of mixing and enthalpy, are negative and exhibit flat minima near the composition $C_{\text{Ti}} = 0.43$. The Al–Ti intermetallic phase was postulated as energetically favored and the preferential arrangements of Al and Ti constituent atoms favor the formation of AlTi-complexes in the liquid alloys.

The optimized data set of the excess Gibbs energy of mixing, G_{M}^{XS}, of Al–Ti liquid alloys [9] together with the Gibbs energy of mixing [10], G_{M}, the enthalpy of mixing [11], and Al-activity data [12,13] have been used to calculate the interaction energy parameters using the CFM. The surface tensions of the pure components, Al [14] and Ti [15], are taken from the literature. Due to their affinity for oxygen, their values exhibit large scatter. Accordingly, it is important to note that, for a different choice of the surface-tension reference data, the calculated values will be different.

The surface tension of Al–Ti molten alloys at 1,700°C is shown in Fig. 9. For this temperature the surface-tension isotherms have been calculated using the CFM, the QCA for a regular solution, as well as the ideal solution model. As can be seen for both surface-tension isotherms, calculated by the CFM and the QCA for a regular solution, they deviate positively with respect to that calculated by the ideal solution model, confirming that liquid alloys with negative excess Gibbs energy in the bulk exhibit positive surface-tension deviations with respect to ideal behavior. The clustering effects on the surface tension and surface segregation are in opposition, and thus the surface-tension isotherm obtained by the CFM is higher than that calculated by the QCA, in agreement with the previous considerations related to Al-segregation on the surface of Al–Ti melts.

Except for the surface-tension data for Al-50at%Ti liquid alloys, there is a complete lack of experimental data. It is interesting to underline that this result agrees very well

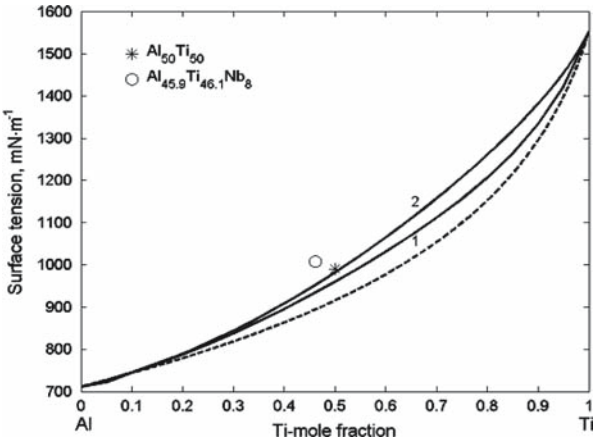

Fig. 9 Surface tension of Al–Ti liquid alloys at T = 1700°C. (1: QCA; 2: CFM, ——: ideal solution). For comparison, the surface tension of the Ti-45.9Al-8Nb alloy is also shown

with the corresponding CFM-calculated value. In order to estimate the effects of a third component on the surface tension, the experimental result for $Ti_{46.1}Al_{45.9}Nb_8$ is also shown. Assuming the Ti-content as constant, at $T = 1{,}700$°C, the surface tension of this alloy is higher with respect to that of Al-50at%Ti due to the contribution of Nb.

3 Summary

Within the IMPRESS project, concerted action was taken to determine the thermophysical properties of a γ-TiAlNb alloy, suitable for casting large turbine blades. Whereas conventional methods worked up to 1,300°C in the solid phase, difficulties were encountered to process the liquid phase in a crucible. This prevented the measurements of specific heat, viscosity, and electrical conductivity in the liquid phase. The density and surface tension of liquid TiAlNb were measured using electromagnetic levitation as a containerless technique. The data obtained are used for subsequent simulation of the casting process.

Acknowledgment This work was carried out under contract FP6-500635-2 of the European Commission.

References

1. D. Jarvis, Mater. World **11** (2005)
2. R. Harding, R. Brooks, G. Pottlacher, J. Brillo, in A. Rosenberger, *Gamma Titanium Aluminides*, ed. by Y. Kim, H. Clemens, (TMS, Warrendale, Pennsylvania, 2003)
3. J. Brillo, I. Egry, Int. J. Thermophys. **24**, 1155 (2003)
4. D.M. Herlach, R.F. Cochrane, I. Egry, H.J. Fecht, A.L. Greer, Int. Mater. Rev. **38**, 273 (1993)
5. D.L. Cummings, D.A. Blackburn, J. Fluid Mech. **224**, 395 (1991)
6. B. Roebuck, M.G. Gee, M. Brooks, D. Cox, R. Reed, in *Component Optimisation from Materials Properties and Simulation Software*, ed. by W.J. Evans, R.W. Evans, M.R. Bache, (University of Wales, Swansea, United Kingdom, 1999), p. 233

7. A.B. Bhatia, R.N. Singh, Phys. Chem. Liq. **13**, 177 (1984)
8. R.N. Singh, Can. J. Phys. **65**, 309 (1987)
9. F. Zhang, S.L. Chen, Y.A. Chang, U.R. Kattner, Intermetallics **5**, 472 (1997)
10. F. Zhang, W. Huang, Y.A. Chang, Calphad **21**, 337 (1997)
11. Yu.O. Esin, N.P. Bobrov, M.S. Petrushevskii, P.V. Gel'd, Russ. Metall. **5**, 86 (1974)
12. M. Maeda, T. Kiwake, K. Shibuya, T. Ikeda, Mater. Sci. Eng. **A239–240**, 276 (1997)
13. N.S. Jacobson, M.P. Brady, G.M. Mehrotra, Oxid. Met. **52**, 537 (1999)
14. G. Lang, P. Laty, J.C. Joud, P. Desré, Z. Metallkd. **68**, 113 (1977)
15. T. Ishikawa, P.-F. Paradis, T. Itami, S. Yoda, J. Chem. Phys. **118**, 7912 (2003)